THE PUBLISHING HOUSE
OF THE ROMANIAN ACADEMY

PROCEEDINGS OF THE ROMANIAN ACADEMY, Series A,
Volume 19, Number 1/2018, pp. 53–60

LASER SCANNERS WITH ROTATIONAL RISLEY PRISMS: EXACT SCAN PATTERNS

Virgil-Florin DUMA[1,2], Alexandru SCHITEA[1]

[1] "Aurel Vlaicu" University of Arad, 3OM Optomechatronics Group, Arad 310130, Romania
[2] "Politehnica" University of Timisoara, Doctoral School, Timisoara 300222, Romania

Corresponding author : Virgil-Florin DUNA, E-mail: duma.virgil@osamember.org

Abstract. We approach the exact scan patterns produced by scanners with rotational Risley prisms. Previous methods have considered such studies mostly approximately, in the paraxial domain or using the third-order theory. Exact, but complicated analytical solutions have also been developed. In contrast, we propose a novel, easy-to-use, graphical method, in order to complete the exact modeling of the scanning process: with a mechanical design program, CATIA V5R20 (Dassault Systèmes, Paris, France). By ray-tracing using the prisms equations, the scan patterns are determined and studied with regard to the characteristic parameters of the device: prism angles and their rotational speeds, as well as the scanner geometry. Marshall's characteristic parameters are utilized: the ratios of the prism angles and of the rotational speeds. An experimental validation of the modeling procedure is completed. The exact modeling method proposed allows for choosing the most appropriate parameters of the device in order to obtain a certain scan pattern for a specific application.

Key words: laser scanners, Risley prisms, rotational wedges, scan patterns, geometrical optics, modeling, multi-parametric analysis, experimental study.

1. INTRODUCTION

Risley prisms [1] are utilized in a variety of applications, including interferometry [2, 3], holography [4], polarimetry [5], attenuation of light [6], precision pointing (for example for satelite positioning [7]), and raster scanning [8–11] – for example in biomedical imaging, for Confocal Microscopy (CM) [12] or Optical Coherence Tomography (OCT) [13]. In the latter they can be an alternative to galvanometer scanners (GSs) [14], polygonal mirror (PM) devices [15], or Micro-Electro-Mechanical Systems (MEMS) [16]. Sometimes they are also coupled with other scanners, for example GSs, in order to achieve not only bi-dimensional (2D), but also tri-dimensional (3D) scanning [17].

Laser scanners with Risley prisms usually consist of a pair of rotational elements [8–11] – in most cases double wedges – but there are also solutions with tilting prisms [18], or combinations of rotational and tilting elements [19]. In order to minimize dispersion, a pair of doublets can be used [20], while for a supplemental degree of freedom in generating scan patterns, devices with three prisms can be employed [21]. The diameter of the prisms ranges from tenths of cm for satelite positioning [7] to sub-milimetric, for endoscopes [22].

With regard to other scanning devices, Risley prisms have specific advantages and drawbacks [13]. Essentially, they provide a fast 2D scanning in a more compact construct than dual axis GSs or PM plus GS systems [1]. Also, both their axial dimension and their diameter can be minimized, and micro-optical solutions can be relatively easily achieved [22]. While their compactness can only be matched by MEMS, their issues are related to their driving solutions and to the complicated patterns of the laser spot that they generate and which need to be followed in order to achieve image reconstruction, for example in CM [12].

In order to determine the equations of their scan patterns, devices with Risley prisms have been studied analitically in the first [8] or in the third order approximation [9], as well as with more complicated exact solutions [10]. Their inverse problem has been approached in order to obtain the position of the prisms that produces an emergent beam in a certain direction [11]. However, the fundamental approach has been done by Marshall, who has proposed, in his seminal work [8], two parameters of these devices to characterize scan

patterns – and we use this practical approach in the present study, as well. However, in [8] only approximate patterns were determined – using the approximation of small prism angles (i.e. for rotational optical wedges).

The aim of the present paper is to provide a method to determine the exact scan patterns – not analitycally, as in previous studies [9–12], but graphically, by ray tracing using a 3D mechanical design program, CATIA V5R20 (Dassault Systèmes, Paris, France). This approach, first proposed in [23], is completed by elements of a multi-parametric study of the scan patterns with regard to the characteristics of the device [24] – to provide users with a fast method to choose the most appropriate scanner parameters in order to satisfy the requirements of a specific application.

In the remaining of this paper, Section 2 presents the Risley prisms scanner. The scan patterns are obtained through modeling and discussed for different parameters of the device in Section 3 – for positive and negative relative rotational speeds of the prisms. Experimental validations of the modeling part are presented, as examples, in Section 4, while Section 5 concludes the paper and points out future work.

2. RISLEY PRISMS SCANNER

From the four possible configurations of scanners with Risley prisms [9, 11], we consider in this study the most convenient one (Fig. 1), with the two surfaces perpendicular on the optical axis (O.A.) placed on the outer sides of the device. The equations of the Risley prisms, in the positions characterized by relative rotation angles $\varphi = 0°$ and $\varphi = 180°$ (Fig. 1b and 1c, respectively) between the two prisms are:

$$\varepsilon_1 = 0;\quad \varepsilon_1' = \varepsilon_1;\quad \varepsilon_2 = \theta_1;\quad n\sin\varepsilon_2 = \sin\varepsilon_2';\quad \varepsilon_2' - \varepsilon_3 = \theta_1 \pm \theta_2; \tag{1}$$
$$\sin\varepsilon_3 = n\sin\varepsilon_3';\quad \mp\varepsilon_3' \pm \varepsilon_4 = \theta_2;\quad n\sin\varepsilon_4 = \sin\varepsilon_4'$$

where θ_1 and θ_2 are the angles of each of the two prisms, considered with the same refractive index n. The first sign in Eqs. (1) and (2) corresponds to the maximum angular deviation D^{max} of the emergent beam (Fig. 1(b)), and the second one to the minimum angular deviation D^{min} (Fig. 1c), therefore:

$$D^{max,\ min,} = \varepsilon_4' = \arcsin\left\{ n\sin\left[\pm\theta_2 + \arcsin\frac{\sin\left[\arcsin\left(n\sin\theta_1\right) - \left(\theta_1 \pm \theta_2\right)\right]}{n} \right] \right\}. \tag{2}$$

For optical wedges, with the small angle approximation, these deviations have the well-known equations: $D^{min,\ max} = (n-1)(\theta_2 \pm \theta_1)$. For the particular case of identical wedges (i.e., for $\theta_1 = \theta_2$), as $D^{min} = 0$, the emergent beam (the dotted line in Fig. 1c) is parallel to the O.A. Its linear deviation from the O.A., necessary in order to verify the modeling, can be easily calculated taking into account the geometry of the scanner in Fig. 1c):

$$\Delta(\theta) = \left(e\cos\theta - a\sin\theta\right)\left(\frac{n\cos\theta}{\sqrt{1-n^2\sin^2\theta}} - 1\right)\sin\theta, \tag{3}$$

where e is the axial dimension of the device (on the z-axis), a is the transversal dimension (on the y-axis), while L is the distance from the final surface of Prism 2 to the screen/scanned plane. In the entire modeling process that follows, the scanner parameters considered are: $e = 15$ mm; $L = 100$ mm; $a = 38$ mm; $n = 1.5$.

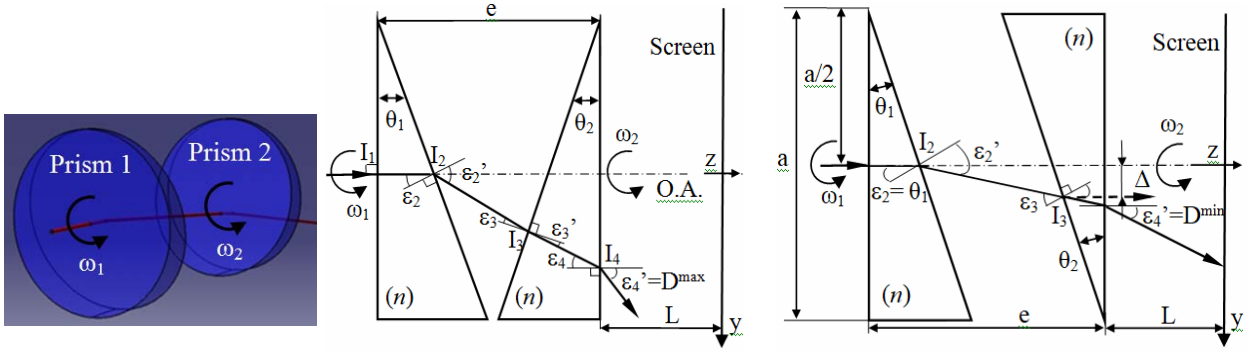

a) b) c)

Fig. 1 – a) Laser scanner with rotational Risley prisms: modeling with a 3D mechanical design program, CATIA V5R20. Two extreme characteristic positions for the device: with a relative rotation angle of 0° (b) and of 180° (c) between the two prisms.

3. EXACT SCAN PATTERNS. MODELING AND ANALYSIS

While analytical approaches prove to be quite complicated [9–11], our proposed modeling method can obtain the scan patterns of this type of device in a simple, fast, and exact manner – the latter aspect in contrast to approximate approaches where such patterns have been obtained as Lissajoux figures – but only in the paraxial domain [8]. Thus, using Eqs. (1) – with no approximations and without vectorial calculus [9-11] – we have obtained the exact trajectories of the laser beam (reduced to a single ray) through the system, by drawing the trajectory of this ray using a mechanical design program, CATIA V5R20 (Dassault Systèmes, Paris, France). The position of the laser spot on a screen situated at the distance L from the scanner (Fig. 1) has been thus determined for each relative position of the two prisms; the scan pattern has been therefore obtained, as shown in the study in Figs. 2–10. This ***multi-parametric analysis*** has been carried out with regard to each characteristic of the scanner, but also by considering Marshall's elegant parameters: k, the ratio of the prisms angles and M, the ratio of the rotational speeds [8]:

$$k = \theta_2 / \theta_1 \qquad \text{and} \qquad M = \omega_2 / \omega_1 . \tag{4}$$

The analysis allows for extracting ***rules-of-thumb*** for the optimal use and design of such devices:

(i) For one of the rotational speeds equals to 0: in this case, when one of the prisms in Fig. 1 is fixed, the other one produces a circular trajectory of the laser spot on the screen – as presented in Fig. 2a for $\omega_2 = 0$ and in Fig. 2b for $\omega_1 = 0$. With regard to the initial angular position of the fixed prism (at 0; 90; 180; 270°), the circular scan pattern produced by the other prism is placed with its center in this corresponding position.

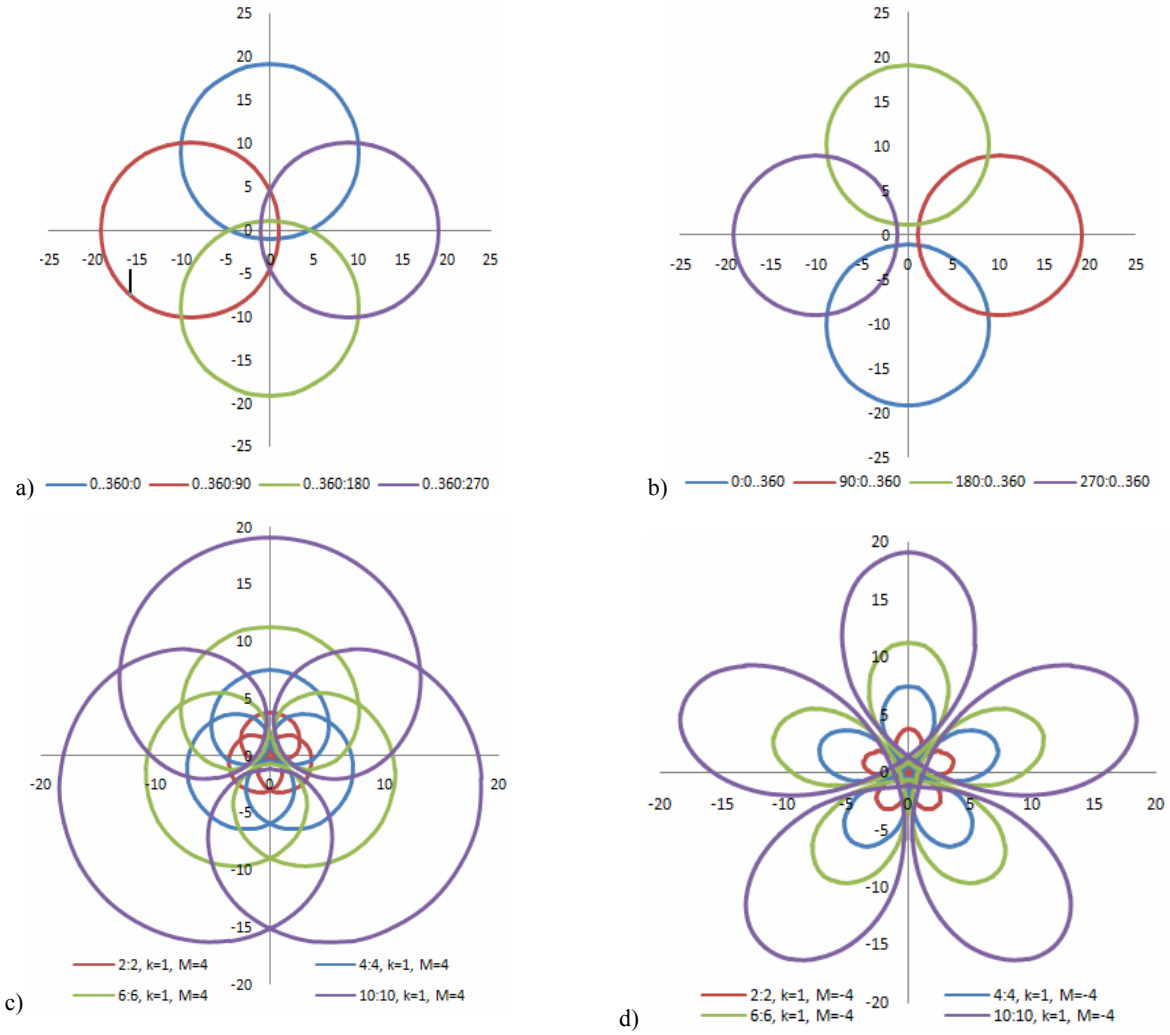

Fig. 2 – Trajectories of the laser spot in the case of a stationary prism: a) for Prism 1 and b) for Prism 2 fixed. Scan patterns for different identical prism angles: $\theta = 2; 4; 6; 10°$ (therefore k = const.; in particular, $k = 1$) and M=const.; c) $M = 4 > 0$ and d) $M = -4 < 0$.

One can remark the difference in the dimensions of the circles in Fig. 2a and b, due to the different axial positions of the two prisms (Fig. 1b): as Prism 1 is placed at a longer distance from the screen, the circles it produces when rotating (see Fig. 2a) are larger.

(ii) For different values of the prism angle θ (considering, for simplicity, in Fig. 2, the two prisms identical): as θ is varied from 2 to 10°, one can see that the shape of the scan patterns is the same, but their dimension is increased almost proportional to θ: it therefore verifies, from Eq. (3), the deviation $D^{max} = 2(n–1)\theta$ obtained for small prism angles. All the parameters except θ have been kept constant: in particular, $k = 1$, while for Fig. 2c, $M = 4 > 0$ and for Fig. 2d, $M = –4 < 0$.

(iii) For another configuration of the Risley prisms (config2, bottom right, Fig. 3a), the difference from the pattern produced by the device in Fig. 1 (config. 1, bottom left, Fig. 3a) is minimal, for the distance $L = 100$ mm considered in the study. These differences between the scan patterns increase with both θ and L.

(iv) For a fractional value of *M*, the scan patterns are 'opened', spiral-like, as shown in Fig. 4 – and as pointed out in studies on approximate patterns [8, 9] or for example on Risley prisms with gratings [25]. For this reason, in this study we work with integer values of M, which provide close, repetitive scan patterns.

(v) For different values of $M > 0$ (and for k = const. = 1, i.e., for two identical prisms, with $\theta_1 = \theta_2 = 2°$) – Fig. 5 – the scan patterns evolve from a circle (for $M = 1$ – when the two prisms rotate together) to trajectories with multiple loops. A good concordance with approximate patterns of such devices is obtained, as the number of loops is $\mu = |M–1|$ [8] – where the modulus has been considered in order to include the next case, of negative ratios of M in the discussion, as well.

(vi) For different values of $M < 0$ – Fig. 6 (for the same value $k = 1$, with $\theta_1 = \theta_2 = 2°$, in order to compare these scan patterns with Fig. 5); the same equation as above is valid for the number of loops of these pattern; this means that for the same value of $|M|$, one has between the number μ of loops $\mu(M < 0) = \mu(M > 0) + 2$.

(vii) For different values of *k*: the patterns are presented for $M > 0$ in Fig. 7, while for $M < 0$, in Fig. 8. The same relationship as the one deduced at the previous point is valid between the numbers μ of loops for $M > 0$ and $M < 0$. For $M > 0$ the patterns evolve with the increase of k from a circle to a pattern with loops and finally, for $M = 6$, to a ring-shaped trajectory with an inner zone with an increasing radius, which is not covered by the laser spot. For $M < 0$ the patterns evolve from a polygon-like shape (Fig. 8a) to a pattern with multiple loops and, for $M = –6$, to the same type of ring-shaped trajectory as for $M = 6$ (but with two more loops).

(viii) The scan patterns can be made to pass through the O.A. – as required by numerous applications (e.g., laser manufacturing), in order to avoid producing the blank inner zone untouched by the laser (Figs. 5 to 8). Thus, for every dimension e and for the same $|M|$, it can be demonstrated through modeling that there is a unique value of L for which this condition is fulfilled, as shown in the examples in Fig. 9.

A *partial validation of the modeling* can be made analytically (while the complete one is made experimentally – Section 4); for example for Figs. 5 and 6, the radius Δ of the inner zone of the patterns is given in these cases, of $k = 1$, by Eq. (3). Thus, for all the patterns in Figs. 5 and 6 (including for the circle in Fig. 5a), Δ equals 0.239 mm – both from modeling and from calculus, the latter using Eq. (3).

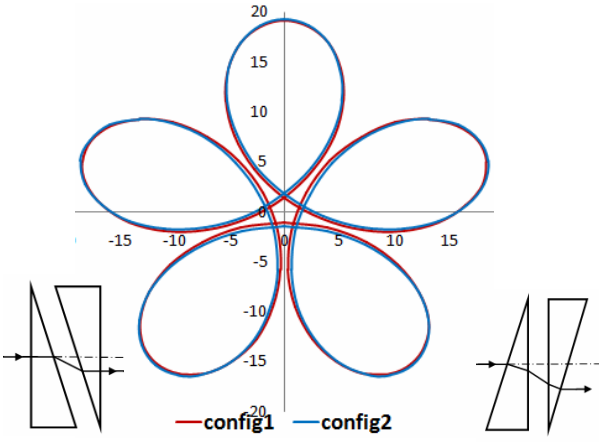

Fig. 3 – Comparison between the scan patterns of two configurations of rotational Risley prisms, for $k = 1$ and $M = –4$.

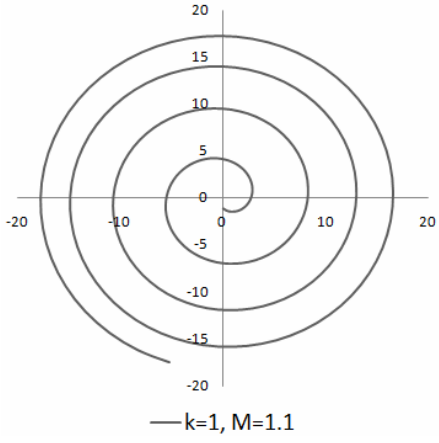

Fig. 4 – Scan pattern of rotational Risley prisms for $k = 1$ and for a fractional value $M = 1.1$.

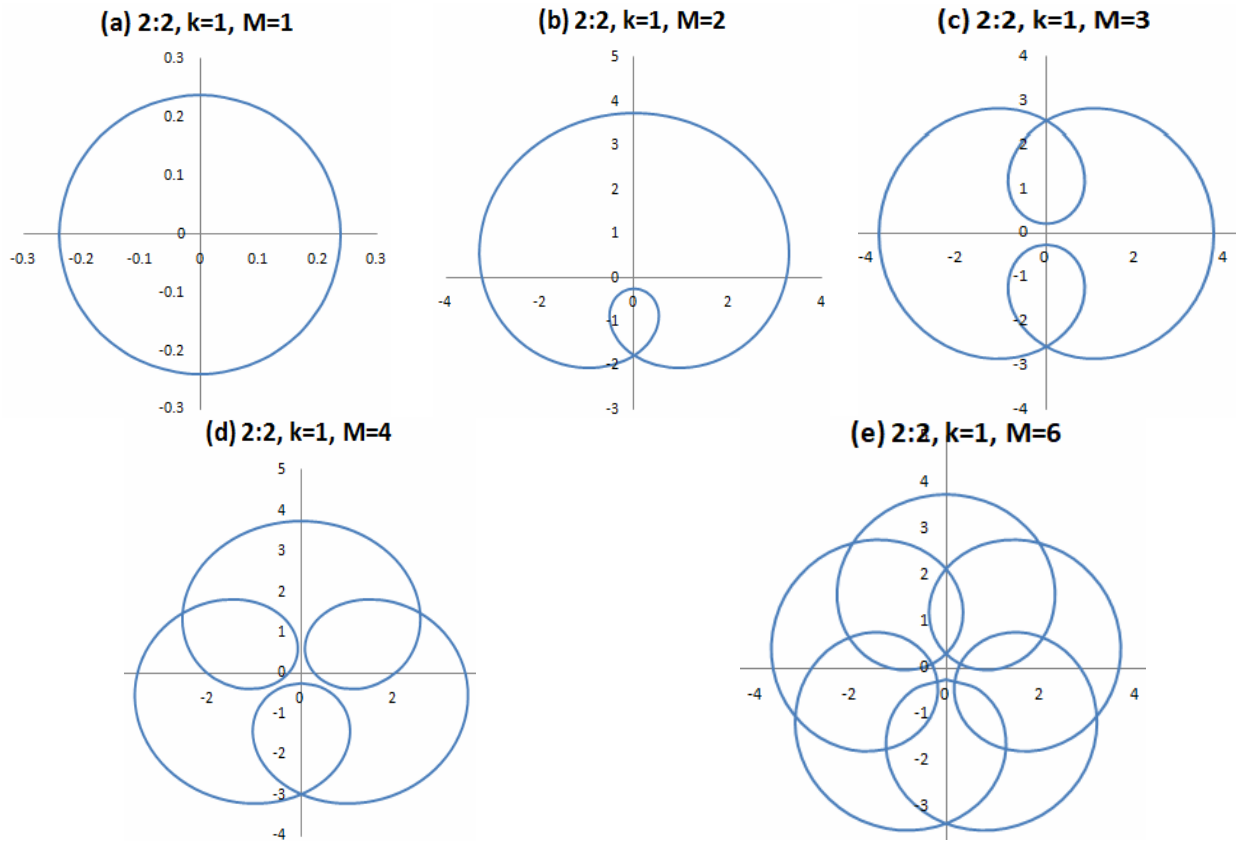

Fig. 5 – Scan patterns of rotational Risley prisms: study with regard to positive values of M (from 1 to 6) – considering k = const. (in particular k = 1), therefore for identical prisms, each one with a prism angle of 2°.

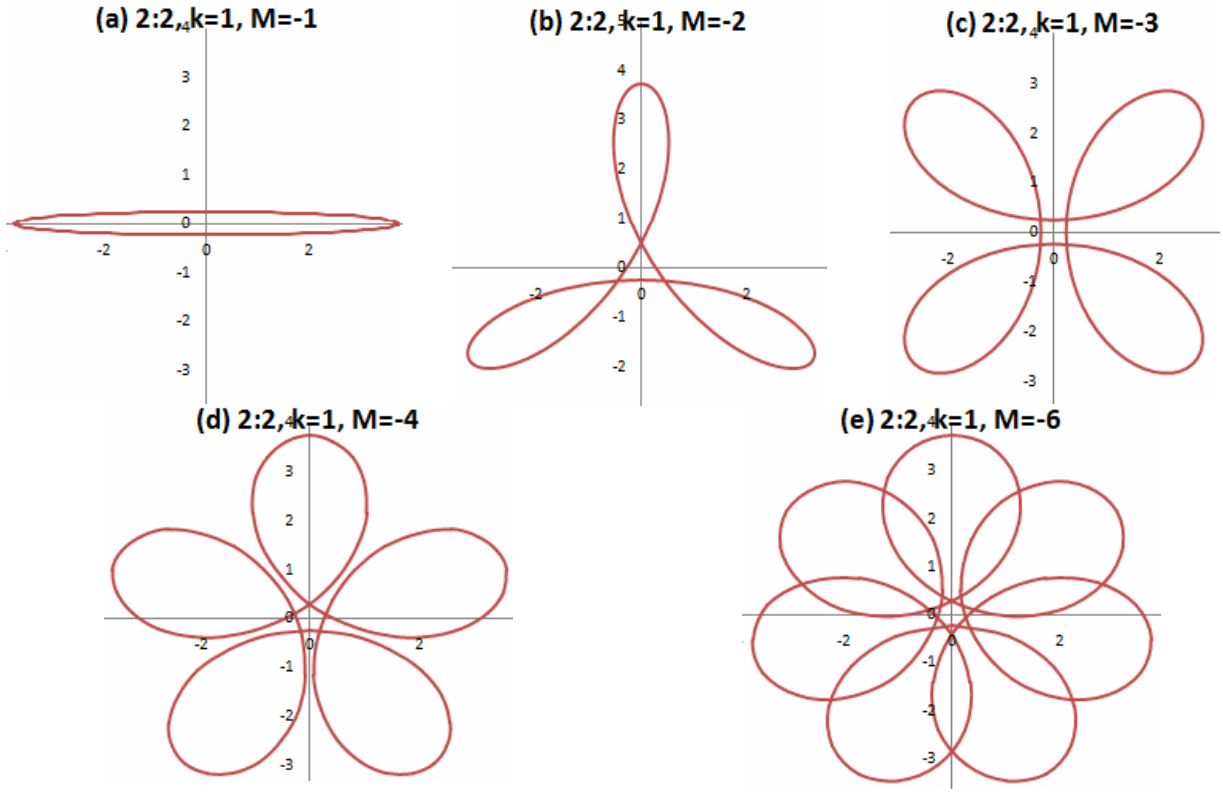

Fig. 6 – Scan patterns of rotational Risley prisms: study with regard to negative values of M (from –1 to –6) – considering k = const. (in particular k = 1), therefore for identical prisms, each one with a prism angle of 2°.

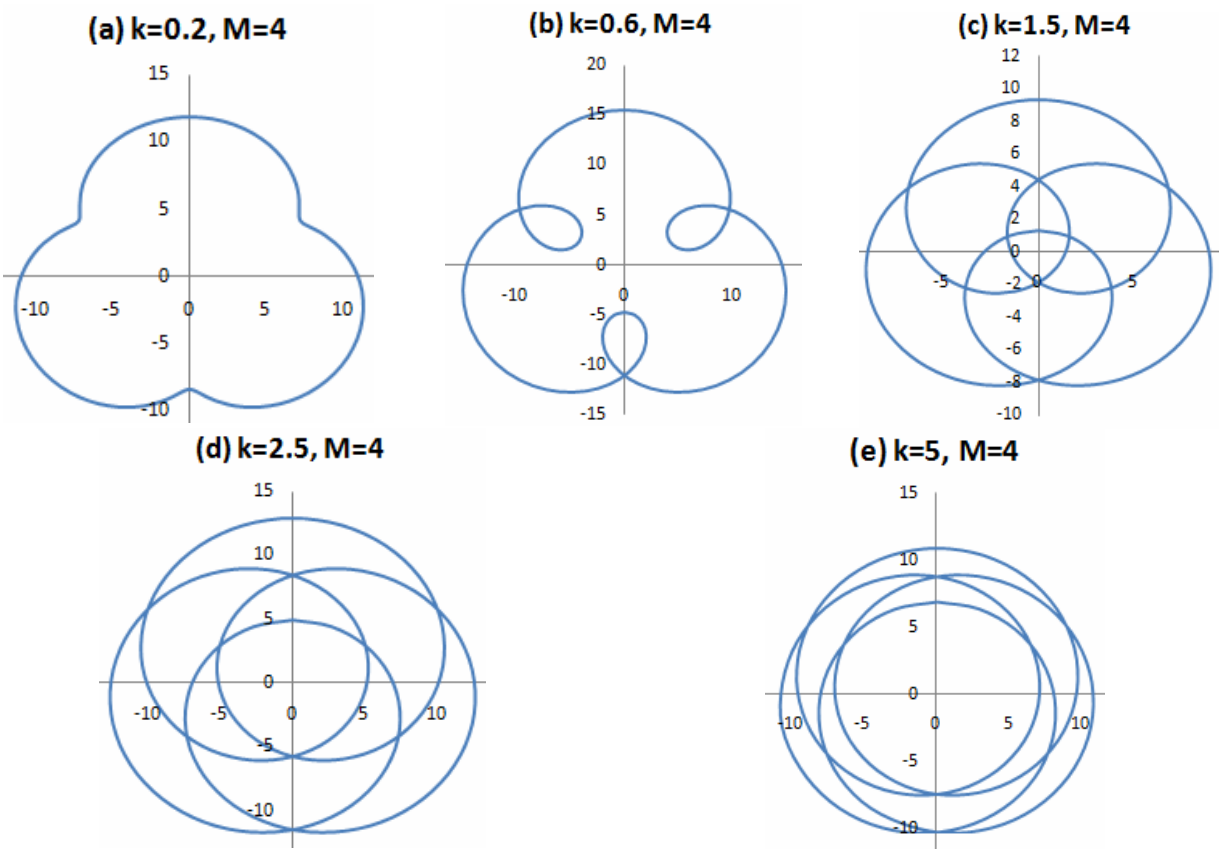

Fig. 7 – Scan patterns of rotational Risley prisms: study with regard to k, considering M = const. = 4 > 0.

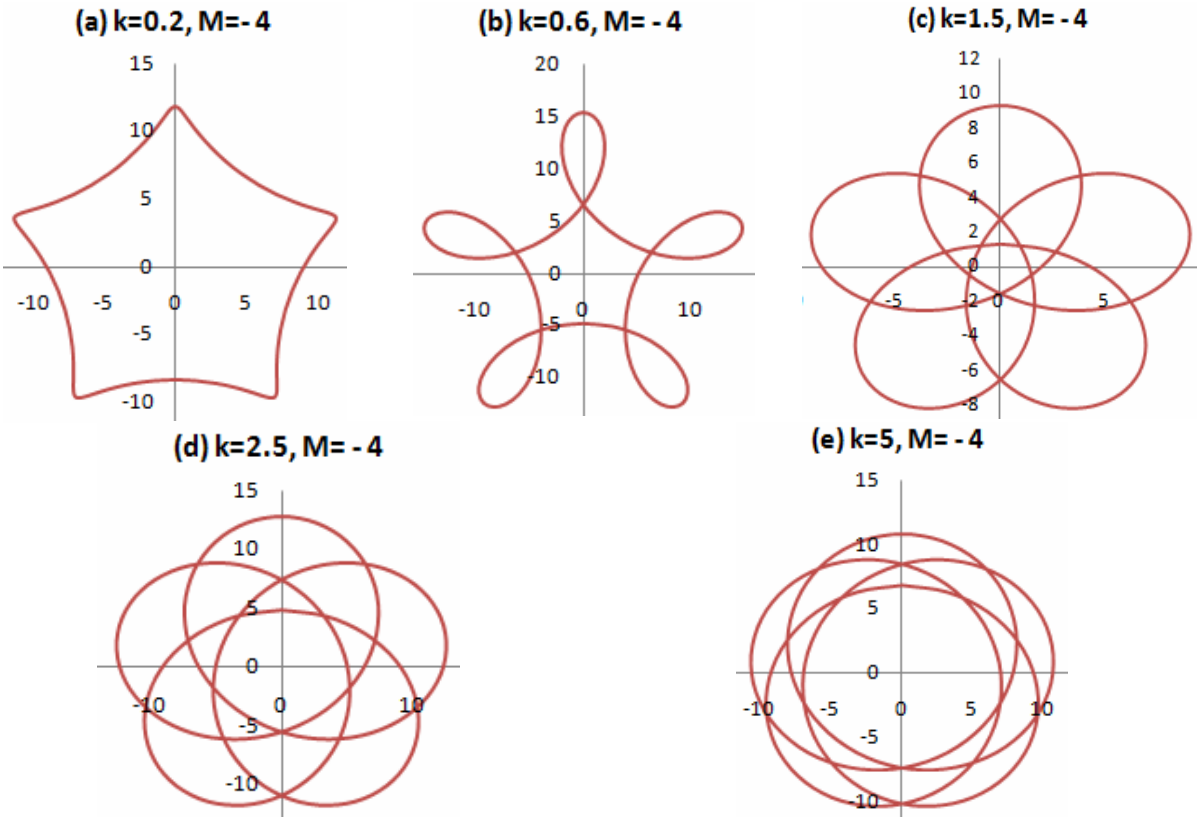

Fig. 8 – Scan patterns of rotational Risley prisms: study with regard to k, considering M = const. = –4 < 0.

Fig. 9 – Ascertainment of the necessary distance L from the scanner to the screen in order to obtain scan patterns that pass through the O.A./z-axis (*i.e.*, through the geometrical center of the scan pattern), for: a) $M = 4$; b) $M = 4$ (both with $k = 5$, value obtained with a pair of prisms with prisms angles of 2° and 5°, respectively).

4. EXPERIMENTAL STUDY

The simple experimental setup designed to verify the results of the modeling is shown in Fig. 10a. The two prisms can be rotated separately, with a precision of 2’ and the well-collimated laser beam is projected through this scanning system on a screen (not shown in the figure). The ratio M of the rotational speeds of the prisms, Eq. (4), is thus simulated by using the different incremental angular movements $\Delta\theta_1$ and $\Delta\theta_2$ of each of the two prisms (where Prism 1 is the one next to the laser): $M = \Delta\theta_2/\Delta\theta_1$.

With regard to the modeling performed, in order to complete a rigorous experimental validation, we have remade a part of the modeling with a deviation angle of 2° for each prism – instead of a prism angle of 2° (as considered in Section 3). With this remark, a good concordance between the modeling and the experimental results has been concluded by comparing the modeled scan patterns (1) and the experimental ones (2) – using a series of characteristic points, as marked in the two examples shown in Fig. 10 for $|M|$ equals 4, with a comparison between the $M > 0$ case (Fig. 10b) and the $M < 0$ case (Fig. 10c).

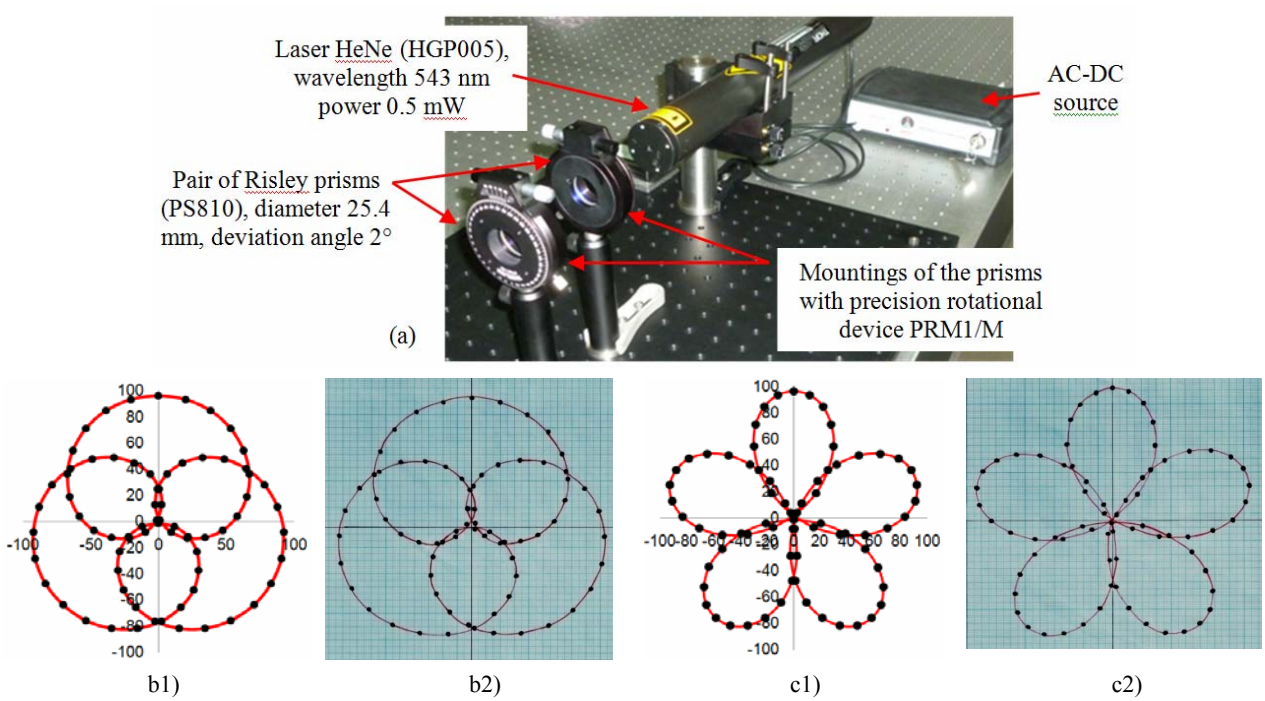

Fig. 10 – a) Experimental setup with (Thorlabs, Newton, NJ, USA) components for the study of the scan patterns of rotational Risley prisms. (b), (c) Scan patterns, modeled (1) and experimental (2), determined for: b) $M = 4$; c) $M = -4$ – with characteristic points considered in order to achieve the validation of the modeling by using the experimental results.

5. CONCLUSIONS

We have proposed in this study a novel, easy-to-use method, based on modeling with a mechanical design program, to obtain the exact scan patterns of laser devices with pairs of rotational Risley prisms. The results of the modeling have been in a good qualitative concordance with previous approximate scan patterns [8], as well as with analytical approaches [9–10] – however, without the difficulties of the latter. A validation with experimental results has also been completed. The analysis of such patterns allows for choosing the appropriate parameters of the scanner in order to satisfy the requirements of a certain application. Future work includes correlations between the exact scan patterns obtained through modeling and analytical aspects of rotational Risley prisms – in their four possible configurations (from which in the present study, due to space limitations, we have approached only one) – as well as to tilting, or rotational and tilting Risley prisms.

ACKNOWLEDGEMENTS

This research was supported by the Romanian National Authority for Scientific Research through CNDI–UEFISCDI Grant PN-III-P2-2.1-PED-2016-1937 (http://3om-group-optomechatronics.ro/).

REFERENCES

1. G.F. MARSHALL, G.E. STUTZ, Eds., *Handbook of optical and laser scanning*, CRC Press, London, 2011.
2. G. GARCIA-TORALES, M. STROJNIK, G. PAEZ, *Risley prisms to control wave-front tilt and displacement in a vectorial shearing interferometer*, Appl. Opt., **41**, pp. 1380–1384, 2002.
3. T. KIYOKURA, T. ITO, R. SAWADA, *Small Fourier transform spectroscope using an integrated prism-scanning interferometer*, Appl. Spectroscopy, **55**, pp. 1628–1633, 2001.
4. Y.-S. CHENG, R.-C. CHANG, *Characteristics of a prism-pair anamorphotic optical system for multiple holography*, Opt. Eng. **37**, 2717, 1998.
5. K. OKA, T. KANEKO, *Compact complete imaging polarimeter using birefringent wedge prisms*, Opt. Express, **11**, pp. 1510–1519, 2003.
6. V.-F. DUMA, M. NICOLOV, *Neutral density filters with Risley prisms: analysis and design*, Appl. Opt., **48**, pp. 2678–2685, 2009.
7. A. LI *et al*., *Radial support analysis for large-aperture rotating wedge prism*, Opt. & Laser Tech., **44**, pp. 1881–1888, 2012.
8. G.F. MARSHALL, *Risley prisms scan patterns*, Proc. SPIE, **3787**, pp. 74–86, 1999.
9. Y. LI, *Third-order theory of the Risley-prism-based beam steering system*, Appl. Opt., **50**, pp. 679–686, 2011.
10. Y. YANG, *Analytic solution of free space optical beam steering using Risley prisms*, J. Light. Tech., **26**, pp. 3576–3583, 2008.
11. Y. LI, *Closed form analytical inverse solutions for Risley-prism-based beam steering systems in different configurations*, Appl. Opt., **50**, pp. 4302–4309, 2011.
12. W.C. WARGER II, Ch.A. DIMARZIO, *Dual-wedge scanning confocal reflectance microscope*, Opt. Lett., **32**, pp. 2140–2142, 2007.
13. V.-F. DUMA, J.P. ROLLAND, A.G. PODOLEANU, *Perspectives of optical scanning in OCT*, Proc SPIE, **7556**, pp. 7556–10, 2010.
14. V.-F. DUMA, P. TANKAM, J. HUANG, J.J. WON, J.P. ROLLAND, *Optimization of galvanometer scanning for Optical Coherence Tomography*, Appl. Opt. **54**, pp. 5495–5507, 2015.
15. V.-F. DUMA, *Polygonal mirror laser scanning heads: Characteristic functions*, Proc. Romanian Acad. A, **18**, *1*, pp. 25–33, 2017.
16. A. COGLIATI *et al*., V.-F. DUMA, J.P. ROLLAND, *MEMS-based handheld scanning probe with pre-shaped input signals for distortion-free images in Gabor-Domain Optical Coherence Microscopy*, Opt. Express, **24**, pp. 13365–13374, 2016.
17. X. TAO, H. CHO, F. JANABI-SHARIFI, *Optical design of a variable view imaging system with the combination of a telecentric scanner and double wedge prisms*, Appl. Opt., **49**, pp. 239–246, 2010.
18. A. LI, W. Yi, Q. ZUO, W. SUN, *Performance characterization of scanning beam steered by tilting double prisms*, Opt. Express, **24**, pp. 23543–23556, 2016.
19. A. LI *et al*., *Laser coarse-fine coupling scanning method by steering double prisms*, Appl. Opt., **51**, pp. 356–364, 2012.
20. C. FLOREA *et al*., *Broadband beam steering using chalcogenide-based Risley prisms*, Opt. Eng., **50**, 033001, 2011.
21. A. LI, X. LIU, W. SUN, *Forward and inverse solutions for three-element Risley prism beam scanners*, Opt. Express, **25**, pp. 7677–7688, 2017.
22. W. PIYAWATTANAMETHA, H. RA, Z. QIU *et al*., *In vivo near-infrared dual-axis confocal microendoscopy in the human lower gastrointestinal tract*, J. Biomed. Opt., **17**, *2*, 021102, 2012.
23. A. SCHITEA, M. TUEF, V.-F. DUMA, *Modeling of Risley prisms devices for exact scan patterns*, Proc. SPIE, **8789**, pp. 8789–40, 2013.
24. V.-F. DUMA, *Risley prisms scanners with different configurations: multi-parametric analysis*, Proc. SPIE, **8925**, 8925 0P, 2014.
25. Y. ZHOU, D. FAN, S. FAN *et al*., *Laser scanning by rotating polarization gratings*, Appl. Opt., **55**, pp. 5149–5157, 2016.

Received June 19, 2017